

LOCALLY WEIGHTED TOTAL VARIATION DENOISING FOR RINGING ARTIFACT SUPPRESSION IN PET RECONSTRUCTION USING PSF MODELING

Arthur Mikhno¹, Elsa D. Angelini^{1,3}, Bing Bai², Andrew F. Laine¹

¹Department of Biomedical Engineering, Columbia University

²Signal and Image Processing Institute, University of Southern California

³Institut Mines-Telecom, Telecom ParisTech, CNRS LTCI, Paris, France

ABSTRACT

Iterative reconstruction with point spread function (PSF) modeling improves contrast recovery in positron emission tomography (PET) images, but also introduces ringing artifacts and over enhancement that is contrast and object size dependent. Mitigation of these artifacts is crucial for clinical and research purposes. In this work we introduce a new iterative regularized reconstruction method that incorporates locally-weighted total variation denoising designed to suppress artifacts induced by PSF modeling. The reconstruction method is evaluated on a simulated cylindrical phantom and preliminary results show that ringing artifacts are suppressed while contrast recovery is maintained.

Index Terms— PET, image reconstruction, point spread function, MLEM, Total Variation

1. INTRODUCTION

Existing and commonly used iterative reconstruction techniques in positron emission tomography (PET) provide a flexible framework for modeling the physics and the scanner geometry, yielding greater image contrast, visual quality and noise robustness than analytical reconstruction methods. Modeling and accounting for the physics of the emissions (e.g. positron range) and the detection processes (e.g. crystal scattering or depth of interaction) is possible by measuring and incorporating the detector point spread function (PSF) into the reconstruction process. Such approach has been shown to improve spatial resolution and image contrast [1]. Unfortunately, it also introduces significant edge artifacts such as over enhancement and Gibbs type of ringing that are both contrast and size dependent (leading to up to 70% overshoot in a cylinder phantom) [2,3]. Mitigation of the above artifacts is crucial to ensure image quantification accuracy, especially since reconstruction with PSF modeling is now implemented and widely used in clinical PET/CT systems.

Some work has been done to characterize and compensate for PSF modeling artifacts. Bai *et al.* showed

that the overshoot depends on region sizes and contrast ratios [2]. Snyder *et al.* observed that the overshoot might be explained by the mismatch between the true and measured PSF [4]. Tong *et al.* reported that ringing frequency and amplitude are related to objects' sizes [5]. A number of different mitigation strategies have been discussed, such as under sampling the PSF and post-filtering the reconstructed images [5]. While these approaches reduce artifacts, they also blur the PET images and undermine the benefits of PSF modeling [4]. Rapisarda *et al.* incorporated a new regularization prior into the reconstruction process that locally modifies the image estimate at each iteration in an attempt to locally control edge enhancement [6]. This method is promising but currently requires optimizing two parameters and while artifacts are suppressed there is loss of contrast recovery.

Total variation (TV) denoising methods have been adapted for Bayesian iterative reconstruction algorithms suitable for use with PET, showing effective suppression of noise and reconstruction of homogenous regions with sharp edges [7]. Previous works assumed a uniform distribution of noise and therefore applied TV globally, which is not suitable for localized PSF modeling artifacts. In this work we develop a new locally-weighted TV strategy, where denoising weights are derived empirically from the data and are incorporated directly into the iterative reconstruction process. We evaluated the proposed reconstruction method on a simulated cylindrical phantom image, assessing contrast and resolution recovery.

2. METHODS

2.1 PET iterative image reconstruction: MLEM algorithm

The maximum likelihood estimate of the PET images is computed using the maximum likelihood expectation maximization (MLEM) algorithm [5]. Following the notation from [6], the MLEM iterative update equation is given as follows:

$$\lambda_b^{k+1} = \frac{\lambda_b^k}{BP_b} \frac{BP_b y_d}{P_d \lambda_b^k} = \lambda_b^k u_b^k \quad (1)$$

where λ_b^k represents the counts in a voxel b within the image

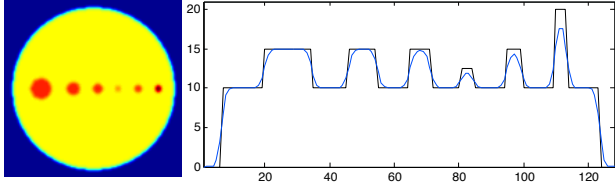


Figure 1. Cylindrical phantom blurred with a 4.5 mm FWHM Gaussian kernel (left) and horizontal profile of pixel intensities through the midline (right) on: the actual phantom (blue line) and the ideal phantom (black line), shown for reference.

λ at iteration k , y_d is the measured projection recorded as number of counts along the line of response (LOR) d , and $\mathbf{1}$ is a unit matrix of the same size as y_d . The forward $P_d(\bullet)_b = \sum [(\bullet)]_b p_{bd}$ and backward $BP_b(\bullet)_d = \sum [(\bullet)]_d p_{bd}$ projectors contain a weight matrix p_{bd} that links the voxel b and LOR d . The term $BP_b \mathbf{1}$ is called the geometric sensitivity, and can be pre-computed prior to reconstruction. Projection terms applied at iteration k can be combined into a multiplicative updating term u_b^k .

2.2. PSF modeling

Following the methodology introduced by Rapisarda *et al.*, incorporating the PSF model into (1) is achieved by modifying the projectors as follows:

$$P_d(\bullet)_b = \sum [(\bullet) * PSF]_b p_{bd} \quad (2)$$

$$BP_b(\bullet)_d = PSF^T * \sum [(\bullet)]_d p_{bd} \quad (3)$$

where PSF represents the PSF kernel and $*$ is a discretized convolution operator as defined in Appendix of [6]. For a symmetric kernel, $PSF = PSF^T$. MLEM reconstruction that utilizes Eq. (2)-(3) will be here referred to as PSF-MLEM.

2.3 Reconstruction software and simulated data

All reconstructions were performed using the STIR open source C++ software (v2.2) [9]. The modified projectors in Eq. (2) and (3) were written in C++ within STIR. A 200mm diameter cylindrical phantom object was simulated, with a background intensity equal to 10, three hot spots of diameter 25mm, 16mm, 12mm with a 1.5:1 contrast ratio (CR), and three 8mm diameter hot spots with CR of 1.25:1, 1.5:1 and 2:1, respectively. The phantom was blurred with a symmetrical 4.5mm FWHM Gaussian kernel [10] to simulate the resolution loss due to physics inherent in the ECAT HR+ scanner (Siemens/CTI) at use in our facility. Figure 1 illustrates the phantom image with resolution and contrast loss due to blurring.

2.4 Total Variation denoising

Following the notations above, at each iteration of Eq. (1) the total variation problem amounts to finding an estimate image $\hat{\lambda}^k$ that satisfies the following optimization problem:

$$\hat{\lambda}^k = \min \frac{1}{2} \left\| \lambda^k - \hat{\lambda}^k \right\|^2 + \beta \left| \nabla \hat{\lambda}^k \right| \quad (4)$$

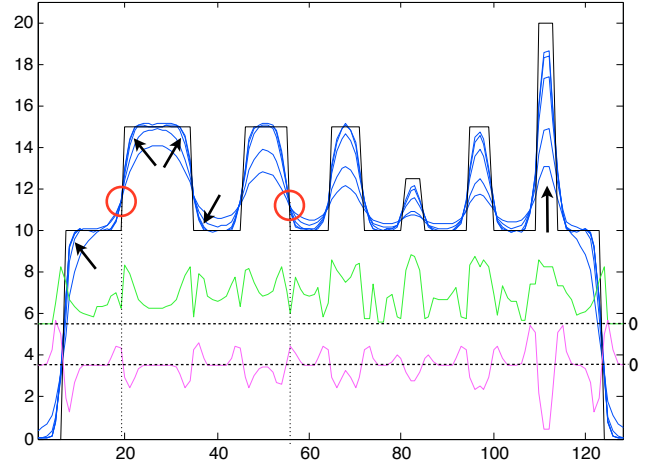


Figure 2. Illustration of how λ^k evolves and its relation with the image structure. Ideal phantom's horizontal midline profile (black line). Reconstructed (MLEM) profiles over several iterations of Eq. 1 (blue lines). Number of iterations to convergence (green line). Second derivative of the blurred phantom's profile (magenta line). Arrows show the dominant direction of evolution of reconstructed profiles over the iterations. Red circles highlight the localization of the inflection points of the reconstructed profiles, which take a relatively small number of iterations to converge.

where $|\cdot|$ and $\|\cdot\|$ are the L_1 and L_2 norms, respectively and β is the regularization weight. TV optimization was performed using the toolbox [7] implemented in Matlab¹.

2.5 Locally-weighted Total Variation denoising

The classical framework given by Eq. (4) minimizes TV over the whole image, while PSF modeling introduces local artifacts. We therefore propose to locally integrate the TV filtered estimate $\hat{\lambda}^k$ into λ_b^k , re-expressing $\hat{\lambda}^k$ as:

$$\hat{\lambda}_b^k = \lambda_b^k + (\hat{\lambda}_b^k - \lambda_b^k) = \lambda_b^k + \Delta \hat{\lambda}_b^k \quad (5)$$

where, $\Delta \hat{\lambda}_b^k = \hat{\lambda}_b^k - \lambda_b^k$, represents the net change in each voxel b on the image estimation after TV denoising. Since TV filtering is only needed at specific voxel locations we propose to locally constrain TV enforcement by introducing a local weight on each TV filtered voxel, defining:

$$\hat{\lambda}_b^k = \lambda_b^k + w_b \Delta \hat{\lambda}_b^k \quad (6)$$

where $\hat{\lambda}_b^k$ is the locally weighted TV estimate and w_b is a spatially-varying weight imposed on the net change of each voxel. Note that if $w_b = 1$ then $\hat{\lambda}_b^k = \hat{\lambda}_b^k$, corresponding to the classical solution to Eq. (4). The PSF-MLEM with TV denoising (TV-PSF-MLEM) algorithm is thus given as follows:

¹ Tremoulheac, Benjamin (2012). Split Bregman method for Total Variation Denoising (<http://www.mathworks.com/matlabcentral/fileexchange/36278>), MATLAB Central File Exchange. Retrieved September 29, 2012

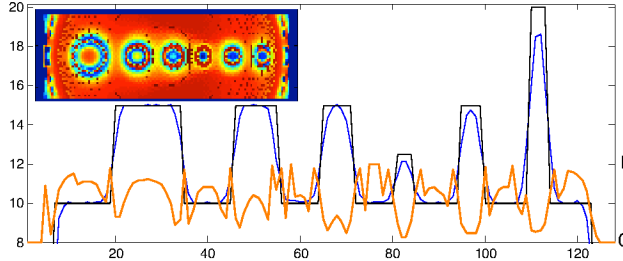


Figure 3. Horizontal profiles through the horizontal midline of ideal phantom (black line), MLEM reconstruction at convergence (blue line) and spatial TV weight w_b (orange line), from the spatial weight map (top left). Left and right axes are for the profiles and w_b , respectively.

For iteration 1 to N:

Step 1: obtain λ_b^{k+1} from λ_b^k using Eq. (1)

Step 2: apply Eq. (4) on λ_b^{k+1} to obtain $\hat{\lambda}_b^{k+1}$

Step 3: apply Eq. (6) on $\hat{\lambda}_b^{k+1}$ to obtain $\hat{\lambda}_b^{k+1}$

Step 4: repeat from Step 1 using $\lambda_b^k = \hat{\lambda}_b^{k+1}$

2.6 Definition of the TV-denoising spatial weights

We needed to design a local weighting scheme such that flat homogenous regions and edges were preserved from the original MLEM estimation, while edge ringing was reduced with TV filtering. Instead of filtering the current estimate relying on its edge maps, we chose a novel approach, to see if we could exploit the information learned on the evolution of λ^k over the iterations of the MLEM reconstruction. Figure 2 shows, on the phantom's horizontal midline profile, the evolution of λ^k over several MLEM iterations (toward convergence), as well as the number of iterations required for each voxel along the profile to converge and the second spatial derivative of the MLEM profile at convergence.

We based our weighting strategy on a few observations: (a) each cylinder's edges have inflection points (defined as zero-crossing of the second spatial derivative) that spatially converge very quickly, (b) the interiors of flat regions converge quickly, while edge refinement continues for a long time (as the peak expands while the support shrinks); (c) the convergence rate for the 8mm cylinders is contrast dependent, and faster for the cylinder with CR 1.25:1 versus 1.5:1, and (d) while the rate of convergence globally mimics the second derivative of the reconstructed profile, there are many local differences. This suggests that there might be unique information contained in the evolution of the MLEM reconstructions that cannot be derived directly from the structure of the reconstructed image.

Based on these observations we designed a new spatial weight w_b as follows:

$$c_b = \min_k \text{abs}(1 - u_b^k) \leq 1e^{-4} \quad (7)$$

$$w_b = 1 - \frac{c_b - \min(c_b)}{\max(c_b - \min(c_b))}$$

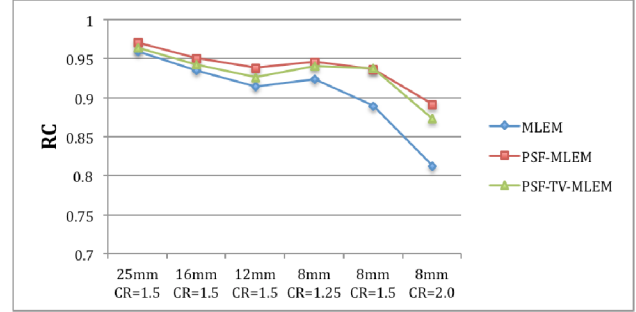


Figure 4. Recovery coefficient (RC) measures for different size cylinders and contrast ratios (CR) of different reconstruction routines. The x-axis reports cylinder diameter (mm) and contrast ratio (CR) relative to the background.

where c_b is defined as the earliest MLEM iteration k in which voxel b converges (in practice when $u_b^k \approx 1$), and w_b is derived by normalizing c_b such that $0 \leq w_b \leq 1$. Figure 3 illustrates the obtained spatial TV-weights w_b .

3. RESULTS

3.1 Evaluation setup on synthetic phantom data

To test whether our spatially weighted TV denoising approach improved image quality, we ran TV-PSF-MLEM empirically setting $\beta = 0.02$. Over several experiments with $\beta = \{.005, .01, .02, .04\}$ we found that $\beta = 0.02$ yielded optimal ringing suppression without degrading image quality. For the MLEM reconstruction, we initialized with $\lambda^0 = 1$. The other reconstructions were initialized with the MLEM estimate.

We quantitatively evaluated contrast recovery using the recovery coefficient (RC) measure, defined as:

$$RC = \frac{\sum_{b \in \Omega_{ROI}} \lambda_b^{recon}}{\sum_{b \in \Omega_{ROI}} \lambda_b^{true}} \quad (9)$$

where the Ω_{ROI} is the region of interest (e.g. inside a cylinder), λ_b^{recon} is the reconstruction being evaluated and λ_b^{true} is the original non-blurred (ideal) phantom. RC measures can be above or below one and $RC=1$ for a perfect reconstruction.

The synthetic cylindrical phantom was reconstructed (200 iterations) with the three different algorithms (MLEM, PSF-MLEM and TV-PSF-MLEM) and the RC values were measured inside each six cylinders. TV-PSF-MLEM yielded better RC measures than MLEM, and only slightly lower than PSF-MLEM, in all cylinders (Figure 4).

3.2 Evaluation of ringing artifacts at edges

To evaluate ringing artifacts, we visually compared the resulting images. For the PSF-MLEM reconstruction, results, illustrated in Figure 5, show that MLEM had no ringing artifact (as expected), PSF-MLEM generates ringing in the background and at edges of the 25mm and 16mm cylinders, as well as over enhancement of the 12mm

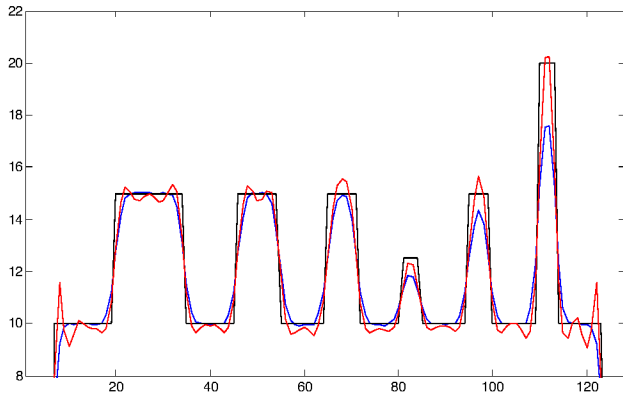


Figure 5. Horizontal midline profile through the ideal (black line), MLEM (blue line) and PSF-MLEM (red line) reconstructions.

cylinder. For the 8mm cylinders there were contrast-dependent over- and under- enhancement.

For the TV-PSF-MLEM reconstruction, results, illustrated in Figure 6, show that ringing artifacts were suppressed on all cylinders edges. The contrast in the 25mm and 16mm cylinders was very well recovered, and over-estimation of the 12mm cylinder intensity was reduced, compared to PSF-MLEM reconstruction (cf. Figure 5). The contrast in the 8mm cylinders was similar for TV-PSF-MLEM and PSF-MLEM reconstructions, demonstrating that locally-weighted TV denoising can suppress ringing within large structures while maintaining the contrast in small regions. In addition to removing ringing artifacts, TV also enforces homogeneity in large regions. This effect is illustrated in Figure 7 in the 25mm cylinder, where MLEM yielded a noisy image, PSF-MLEM induced heterogeneity and ringing at the edge, while TV-PSF-MLEM prevented the ringing and enforced homogeneity inside the cylinder.

4. CONCLUSIONS

We introduced TV denoising in the PSF-MLEM iterative reconstruction method for PET images. This method was evaluated on a synthetic phantom image with multiple cylinders varying in size and contrast. Results showed that TV-PSF-MLEM maintains the good contrast recovery properties of PSF-MLEM while reducing ringing artifacts at edges.

These results are promising, but remain preliminary and need to be investigated further on more complex synthetic phantoms. Indeed, the proposed reconstruction method needs to be evaluated in objects with greater variations in size and contrast and including negative contrast (i.e. cold spots). Robustness with respect to the presence of Poisson noise in the sinogram should also be evaluated. Regarding the methodology itself, the influence of the TV parameter β needs to be studied, and we need to derive stopping criterions of the reconstruction process optimized separately for each of the reconstruction approaches, instead of using the same fixed number of iterations. Finally, further characterization of the proposed reconstruction method using a physical phantom will be the subject of future work.

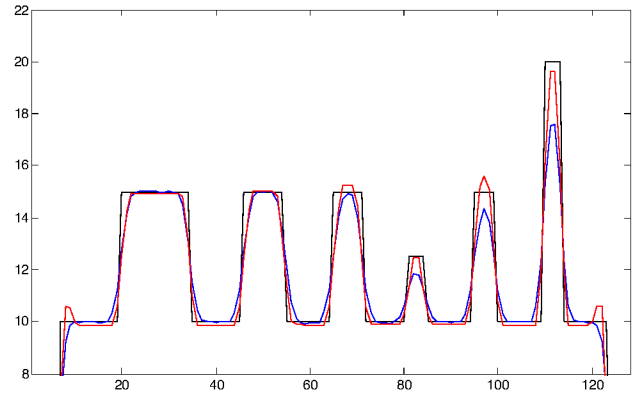


Figure 6. Horizontal midline profile through the ideal (black line), MLEM (blue line) and TV-PSF-MLEM (red line) with $\beta=0.02$ reconstructions.

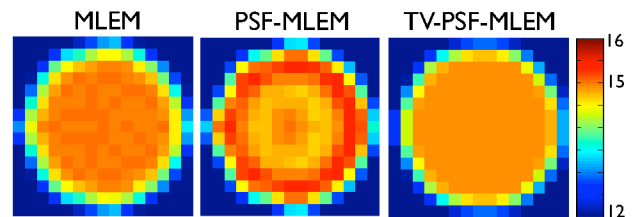


Figure 7. Images of the 25mm cylinder with three reconstructions (MLEM, PSF-MLEM, TV-PSF-MLEM). TV-PSF-MLEM removes PSF-related ringing artifacts and restores homogeneity and contrast level that is similar to true phantom.

5. REFERENCES

- [1] F. C. Sureau, et al., "Impact of Image-Space Resolution Modeling for Studies with the High-Resolution Research Tomograph," *Journal of Nuclear Medicine*, vol. 49, no. 6, pp. 1000–1008, May 2008.
- [2] B. Bai and P. D. Esser, "The effect of edge artifacts on quantification of Positron Emission Tomography," in *Nuclear Science Symposium Conference Record (NSS/MIC)*, 2010 IEEE, 2010, pp. 2263–2266.
- [3] K. Thielemans, et al., "Impact of PSF modelling on the convergence rate and edge behaviour of EM images in PET," in *Nuclear Science Symposium Conference Record (NSS/MIC)*, 2010 IEEE, 2010, pp. 3267–3272.
- [4] D. L. Snyder, et al., "Noise and edge artifacts in maximum-likelihood reconstructions for emission tomography," *IEEE Trans Med Imaging*, vol. 6, no. 3, pp. 228–238, 1987.
- [5] S. Tong, A. et al., "Properties and Mitigation of Edge Artifacts in PSF-Based PET Reconstruction," *IEEE Transactions on Nuclear Science*, vol. 58, no. 5, pp. 2264–2275, Oct. 2011.
- [6] E. Rapisarda, et al., "Evaluation of a New Regularization Prior for 3-D PET Reconstruction Including PSF Modeling," *IEEE Transactions on Nuclear Science*, vol. 59, no. 1, pp. 88–101, Feb. 2012.
- [7] M. Yan, "EM-type algorithms for image reconstruction with background emission and Poisson noise," *Advances in Visual Computing*, pp. 33–42, 2011.
- [8] L. A. Shepp and Y. Vardi, "Maximum likelihood reconstruction for emission tomography," *Medical Imaging, IEEE Transactions on*, vol. 1, no. 2, pp. 113–122, 1982.
- [9] K. Thielemans, et al., "STIR: software for tomographic image reconstruction release 2," *Physics in Medicine and Biology*, vol. 57, no. 4, pp. 867–883, Feb. 2012.
- [10] J. E. Mourik, et al., *Journal of Cerebral Blood Flow & Metabolism*, vol. 30, no. 2, pp. 381–389, Oct. 2009.